



DEM Study of Shear Band Formation in Granular Materials under True Triaxial Test Conditions

Hadi, A.H.¹  and Mirghasemi, A.A.^{2*} 

¹ M.Sc. Student, School of Civil Engineering, College of Engineering, University of Tehran, Tehran, Iran, (Currently Ph.D. Candidate, Department of Maritime and Transport Technology, Faculty of 3ME, Delft University of Technology, Delft, the Netherlands).

² Professor, School of Civil Engineering, College of Engineering, University of Tehran, Tehran, Iran.

© University of Tehran 2022

Received: 19 Jul. 2021;

Revised: 14 Nov. 2021;

Accepted: 04 Dec. 2021

ABSTRACT: Subjected to external loads, granular materials experience severe deformation in a narrow zone before their failure. This phenomenon, which is called strain localisation or shear band, is of vital importance in assessing the stability of the geotechnical structure, studying the stress-strain behaviour of soil and rock materials, and analysing the interaction of soil and structure. The present study is aimed to investigate the effect of various factors on the pattern and inclination of shear band in a general three-dimensional condition of stress using the Discrete Element Method (DEM). Several tests were simulated using a developed version of the TRUBAL program called GRANULE. The GRANULE code was further developed to add the capability of carrying out simulations with different intermediate principal stresses and modelling specimens containing non-spherical particles. The shear band was detected by tracking the motion of the particles and plotting the rotation distribution of particles within the sample. The results prove that the shear band inclination and its pattern, are greatly affected by intermediate principal stress, particle shape, and confining stress. Moreover, it was observed that the change in the b value plays a key role in the alteration of the 3D configuration of the shear band.

Keywords: Discrete Element Method, Granular Materials, Shear Band, Strain Localisation, True Triaxial Test.

1. Introduction

A shear band is defined as the localisation of shear deformations in a set of narrow zones. In other words, a shear band is a thin layer along which two rigid blocks move at different velocities (i.e., strain rates). This phenomenon frequently occurs in granular

materials and is considered one of the failure mechanisms in granular media. For instance, localised failure of granular soils in the form of shear bands may lead to several known geotechnical failures. Thus, the deformation and strength properties of the geotechnical structures are controlled by the soil behaviours inside the shear band

* Corresponding author E-mail: aghasemi@ut.ac.ir

(Desrues and Viggiani, 2004). This indicates the great importance of accurate estimation of the shear band formation in geotechnical problems. In recent years, a great number of theoretical, experimental, and numerical studies have been conducted to estimate the occurrence of the shear band and investigate its fundamental mechanisms.

Two distinctive failure mechanisms have been observed in the geomaterials, namely diffusive and localised instabilities. Diffusive instability may occur before the localised one and are mostly observable in undrained conditions (Mukherjee et al., 2017; Alipour and Lashkari, 2018; Lashkari et al., 2019). From a theoretical standpoint, localised failure can be considered as instability caused by the bifurcation of the uniform deformation of a soil structure (Rudnicki and Rice, 1975). Put differently, shear band initiation highly depends on the pre-localisation characteristics of homogeneous deformation. Mathematically, the shear band initiation occurs due to the non-uniqueness of equilibrium equations in a particular constitutive model (Gu et al., 2014). Such theories have accurately forecasted shear band occurrence based on Cosserat continuum theory (Vardoulakis, 1989) and elasto-plastic constitutive models (Bardet and Proubet, 1991). However, Desrues and Viggiani (2004) indicated that the theoretical and numerical approach based on continuum mechanics has inherent limitations for studying the mechanical behaviour of granular soils.

In addition to the theoretical studies regarding the investigation of shear band in granular materials, several laboratory experiments have been carried out using advanced equipment like stereophotogrammetry (Desrues and Viggiani, 2004), X-ray Computed Tomography (Andrade et al., 2012), and Particle Image Velocimetry (PIV) (Lashkari and Jamali, 2021). According to these extensive experimental works, the shear band formation and its characteristics are

influenced by many factors such as the density, inherent and stress-induced anisotropy of the material, the confining stress, shape of the material, and the particle size.

Nevertheless, these experimental methods cannot provide all the important details of the shear band such as particle rotation, void ratio, and contact force. Additionally, the fundamental mechanism explaining the shear band formation, and the way the characteristics of the shear band are affected is not well understood yet. From the micromechanics point of view, granular media are composed of particles and the macroscale behaviour of the assembly is the result of microscale particle interactions through contacts. Therefore, the contact-based microstructure of the granular materials, such as contact force, contact number, and particle distributions, may play a critical role in determining macroscopic behaviour. The Discrete Element Method (DEM), initially introduced by Cundall and Strack (1979), is a powerful alternative employed by numerous researchers to investigate the micro-, meso-, and macroscale behaviour of granular media in various fields (Yan et al., 2015; Kildashti et al., 2018; Mohajeri et al., 2018; Hajiazizi and Nasiri, 2019; Nadimi et al., 2019; Ghassemi and Shahebrahimi, 2020; Salimi and Lashkari, 2020; Bayesteh and Hoseini, 2021; Fransen et al., 2021). Although DEM is mainly utilised to study particulate assemblies, it has also been used to investigate the microscale properties of clays (Jaradat and Abdelaziz, 2019; Khabazian et al., 2020). Needless to say, shear banding, a common phenomenon in granular media, has been extensively studied using DEM (Garcia and Bray, 2019; Tang et al., 2019; Yu et al., 2021). For instance, Bardet and Proubet (1991) performed DEM simulations to study the structure of the shear band. Their results showed that as the axial strain increases progressively, the thickness of the shear band declines from 9 to 7.5 times the mean particle diameter. Also, they showed the

importance of particle rotation in the shear band. However, they performed their simulation on circular particles that have no rolling resistance at contacts. Iwashita and Oda (1998) used rolling resistance at contact in the DEM and identified that the shear bands' development can be effectively simulated only when incorporating the rolling resistance at contacts in the DEM. Jiang et al. (2010) carried out some 2D numerical simulations on circular disks and realised that the thickness of the shear band is 10-14 times the average particle diameter. Also, contrary to the results by Bardet and Proubet (1991), they realised that this thickness rises as the axial strain increases. Another noteworthy result of this study is that shear band inclination decreases in the range of 54° to 50° with increasing axial strain which can be predicted using the Mohr-Coulomb theory. More recently, Tian et al. (2020) have conducted some biaxial simulations to investigate the effect of particle shape on the shear band properties using the aspect ratio (AR). They concluded that the decrease in the AR leads to more inclination of the shear band.

As can be seen in the literature, few researchers have addressed the issue of shear banding in the general three-dimensional conditions of stress, and there is still a need for thorough investigations of how shear band characteristics are affected by various factors. More specifically, there is no past research capturing the 3D configuration of shear band in true triaxial test conditions and addressing how shear band characteristics are influenced by 3D particle shape indices, i.e., angularity and sphericity. In the current study, the effect of particle shape, intermediate principal stress, and confining stress on shear banding in true triaxial test conditions was investigated. To this end, a macroscopic investigation was conducted to understand and explain the deformation process and shear bands' evolution in granular materials. This approach integrates the results of microscopic numerical models

with macroscopic expression in a three-dimensional space. In this regard, the mechanical behaviour of granular materials in the true triaxial test is examined and shear band failure modes are extracted.

2. DEM Modelling

The Discrete Element Method (DEM) is a numerical method intensively employed by researchers to simulate granular materials because of its unique feature of considering interactions between individual particles (O'Sullivan, 2011). In this study, ASTON version of the TRUBAL program called GRANULE (derived from Cundall's DEM code, Trubal Version 1.51: 9, May 1989) which is an open-source code was used to investigate the shear band and the effect of intermediate principal stress as well as the shape of the particles. The most important advantage of GRANULE over the traditional TRUBAL code is its capability to simulate specimens with rigid boundaries. Rigid boundaries are adopted in this study since the experimental work by Lade and Wang (2001) and Ochiai and Lade (1983) were used as benchmarks, and both studies used the true triaxial apparatus developed by Lade (1978) which is equipped with rigid boundaries. Moreover, as stated by O'Sullivan (2011), simulated specimens with rigid boundaries better represent the real physical test compared to periodic boundaries. Cubical samples were simulated to represent the true triaxial apparatus, which is suitable to investigate the effect of the intermediate principal stress on the granular materials. However, the original code was limited to model spherical particles and also, was not capable of performing tests with different b values ($b = (\sigma_2 - \sigma_3)/(\sigma_1 - \sigma_3)$, where $\sigma_1, \sigma_2, \sigma_3$ are principal stresses). Thus the code was further developed to fit our purposes.

2.1. Particle Shape Considerations

In recent years, there have been considerable advances in modelling particles with real shape (Angelidakis et al., 2021a; 2021b; Zhao and Zhao, 2021).

However, for the purpose of simplicity, the multi-sphere method was adopted in this study to generate irregularly shaped particles. In order to quantitatively investigate the effect of particle shape on the mechanical behaviour of the assemblies, the Angularity Index (AI) as introduced by Sukumaran and Ashmawy (2001) and the sphericity index (SPH) proposed by Krumbein (1941) were used. The Angularity Index (AI) for a 3D particle is calculated based on the weighted average of 2D angularities as:

$$AI = \frac{\sum_{k=1}^3 (Ang_k \cdot Area_k)}{\sum_{k=1}^3 Area_k} \quad (1)$$

where AI : is the 3D angularity of the irregularly shaped particle in degree, k : corresponds to different 2D views (i.e., front, top and side views), $Area$: is the area of the 2D projected views, and Ang : is the angularity of the 2D views of the particle which is defined as:

$$Ang = \frac{\sum_{i=1}^N (\beta_{i,particle} - 180)^2 - \left(\frac{360}{N}\right)^2}{3 \times 180^2 - \left(\frac{360^2}{N}\right)} \quad (2)$$

where N : is the number of sharp corners of the 2D image and β_i : is shown in Figure 1.

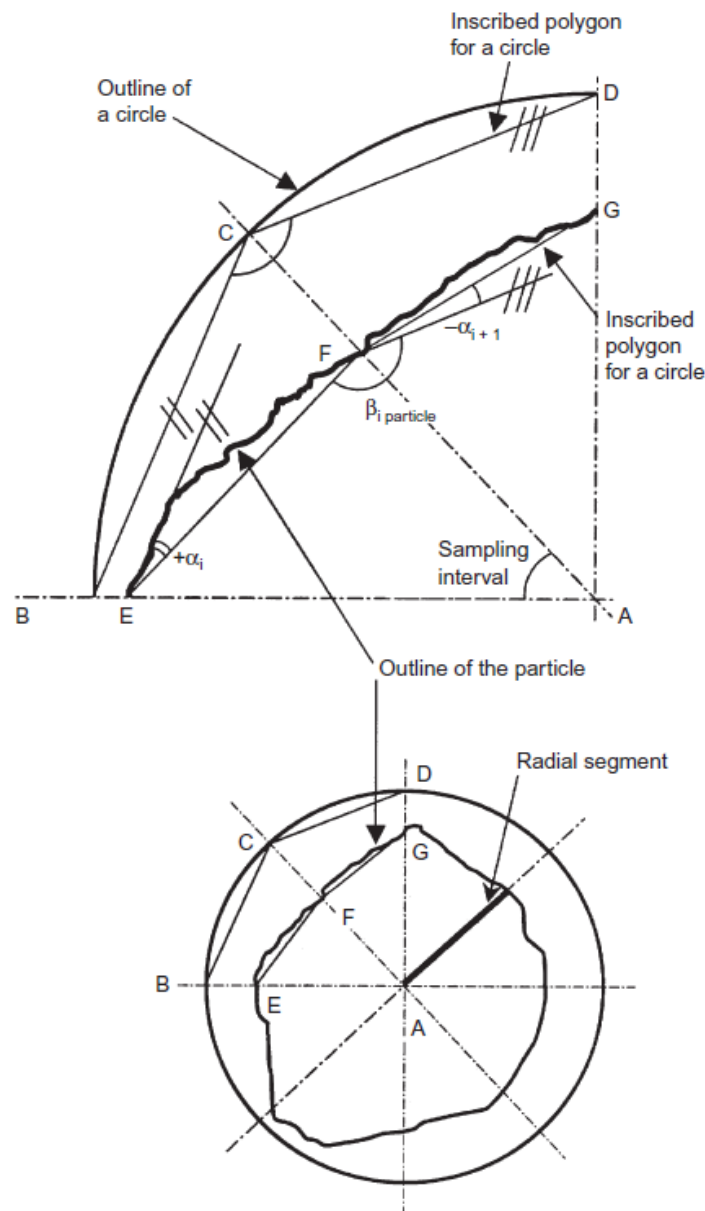


Fig. 1. Parameters used for calculation of 2D angularity (Sukumaran and Ashmawy, 2001)

The sphericity index is also calculated as:

$$\psi = \sqrt[3]{\frac{b \cdot c}{a^2}} \quad (3)$$

where the amount of a , b and c is measured as shown in Figure 2. To this end, the longest dimension of the particle (a in Figure 2) is measured first. Then, the greatest dimensions in two perpendicularly projected planes (b and c in Figure 2) are found afterwards.

The angularity and the sphericity of the particles used in the current study are according to Table 1.

2.2. Contact Detection Algorithm for Irregular Particles

The non-spherical particles used in this study are composed of 4 sub-spheres as illustrated in Table 1. When considering modelling irregularly shaped particles in a DEM code, the central problem of contact

detection arises. A two-step algorithm for detecting contacts between the non-spherical particles. In summary, the first step involves detecting contact between the imaginary bounding spheres containing the whole volume of the irregularly-shaped particles and if any contact was detected, the program would search for the potential contacts between the sub-spheres (Figure 3a). For detailed information about this algorithm, the readers are referred to (Shamsi and Mirghasemi, 2012).

2.3. Calculation of Contact Force and Moment

After completion of the contact detection process, forces and moments of all contacts are calculated. For this purpose, the linear contact law was used in this study. A simple formulation could be presented as follows (O’Sullivan, 2011):

$$dF_n = K_n \cdot dv_n \cdot \Delta t \quad (4)$$

$$dF_s = \min \{K_s \cdot dv_s \cdot \Delta t, \mu \cdot dF_n\} \quad (5)$$

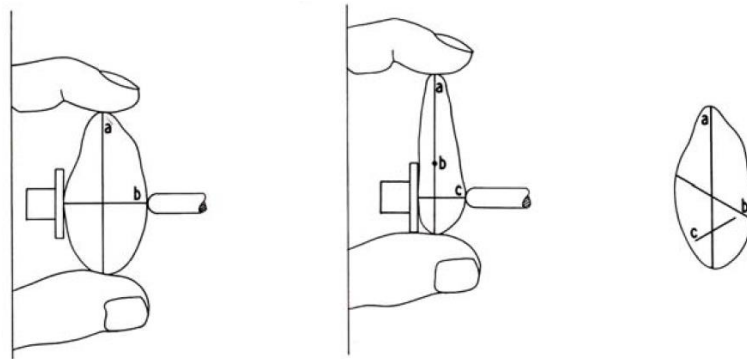
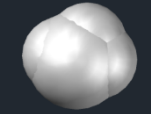
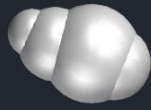


Fig. 2. Definition of the parameters for the calculation of SPH (Krumbein, 1941)

Table 1. Characteristics of particles used in simulations

Particle shape	Particle ID	Sphericity	Angularity (degree)
	P1	100%	0
	P2	93%	8
	P3	70%	15

where, dF_n and dF_s : are the incremental normal and shear force for each cycle, K_n and K_s : are coefficients of normal and shear contact stiffness, dv_n and dv_s : are the normal and tangential components of the relative velocity of particles at the contact point, respectively. μ : is also the coefficient of friction and Δt : is the time step and is computed as:

$$\Delta t = frac \sqrt{\frac{m_{min}}{K_{max}}} \quad (6)$$

where K_{max} : is the maximum of K_n and K_s , m_{min} : is the smallest mass among particles, and $frac$: is a coefficient between zero and one and should be small enough to ensure the numerical stability in the computations. In the simulation, the value of $frac$ was set to 0.33 based on a trial and error procedure.

As the normal and shear forces for each contact are determined, the accumulative force and moment for each sub-sphere (e.g., sphere A in Figure 3) will be determined as:

$$F_{i,sphA} = F_n n_i + \varepsilon_{ijk} F_s \quad i = 1,3 \quad (7)$$

$$n_i = \frac{u_i^B - u_i^A}{d} \quad (8)$$

$$M_{sphA} = R_{sphA} \cdot F_{si} \quad (9)$$

where, F_i : is the resultant force transmitted to the centre of each sub-sphere, u_i : is the centre coordinates of the sub-spheres involved in the contact, d : is the distance between the centre of two sub-spheres, and R : is the radius of the sub-sphere. Once the calculation of force and moment of all the sub-spheres is done, these forces and moments are transferred to the centre of mass of the irregular particle. The total amount of force and moment of a particle is determined using the following equations:

$$(F_{i,particle}) = \sum_{j=1}^{nsph} (F_{ij}) \quad i = 1,3 \quad (10)$$

$$(M_{i,particle}) = \sum_{j=1}^{nsph} (M_{ij}) - \sum_{j=1}^{nsph} (F_{ij}) \cdot r_{ij} \quad i = 1,3 \quad (11)$$

where F_{ij} and M_{ij} : are the total force and moment of each sphere, respectively, $nsph$: is the number of spheres making up the particle, and r_j : is the distance between the centre of the sphere and the centre of the mass of the irregularly shaped particle.

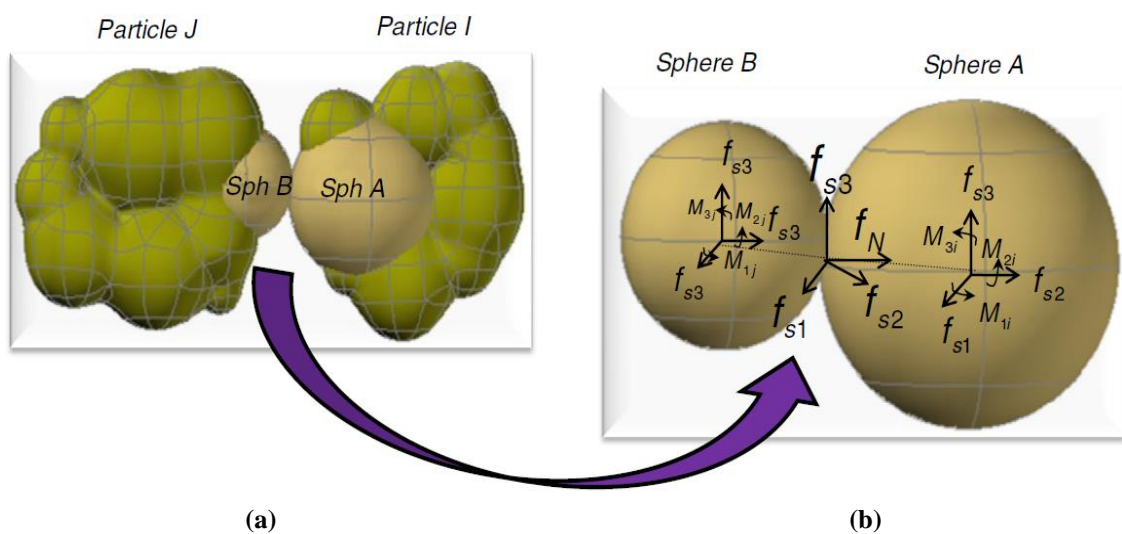


Fig. 3. a) Two sub-spheres in contact; and b) calculation and transfer of forces and moments between two sub-spheres in contact (Shamsi and Mirghasemi, 2012)

2.4. Assembly Properties

The number of particles in a real (and even small) granular assembly is very large. For instance, there are about 4 million particles in a cylindrical sample of sand with a height of 60 mm and a diameter of 30 mm. Simulation of tests using the discrete element method with this number of particles would be extremely time-consuming. Therefore, a much smaller number of particles should be considered. Chantawarangul (1994) compared the results of simulations on samples containing 300, 1000, 3000, and 10000 spherical particles, and concluded that the increase in the number of particles only reduces the oscillation of the curves while the general trend remained unchanged. Taking the time constraint and limited computing power into account, polydisperse assemblies of 2300 clumped particles with the same grain distribution as in Figure 4 were used in the present study.

In order to capture the energy dissipation of a real granular system, three types of damping systems, namely frictional damping, global damping and contact damping were used in this study. Frictional damping prohibits the tangential force from exceeding the frictional strength at the contact between two particles or between particles and walls. Global damping can be imagined as a damper that fixes the particle to a fixed point, and contact damping works

based on the relative velocity of two particles in contact.

The value of parameters used in the current study is listed in Table 2. These values were initially chosen based on what was successfully calibrated against experimental results in the previous study by Danesh et al. (2020) employing the same code, i.e., the GRANULE program. Then, final values were fixed adopting the unbalanced force index (I_{uf}), introduced by Ng (2006), as the main criterion. I_{uf} is defined as:

$$I_{uf} = \sqrt{\frac{\sum_1^{N_b} (\text{unbalanced forces})^2 / N_b}{\sum_1^{N_c} (\text{contact forces})^2 / N_c}} \quad (12)$$

where N_b and N_c : are the number of particles and the number of contacts, respectively. This index should be small enough, i.e., lower than 0.01 in this study, to ensure the numerical stability of the simulation in the sample shearing. Figure 5 shows an example of the unbalanced force index measured at different axial strains with the parameter of Table 2, where I_{uf} was satisfactorily obtained lower than 0.01. In order to better compare the results, all the parameter values are kept unchanged for all simulations.

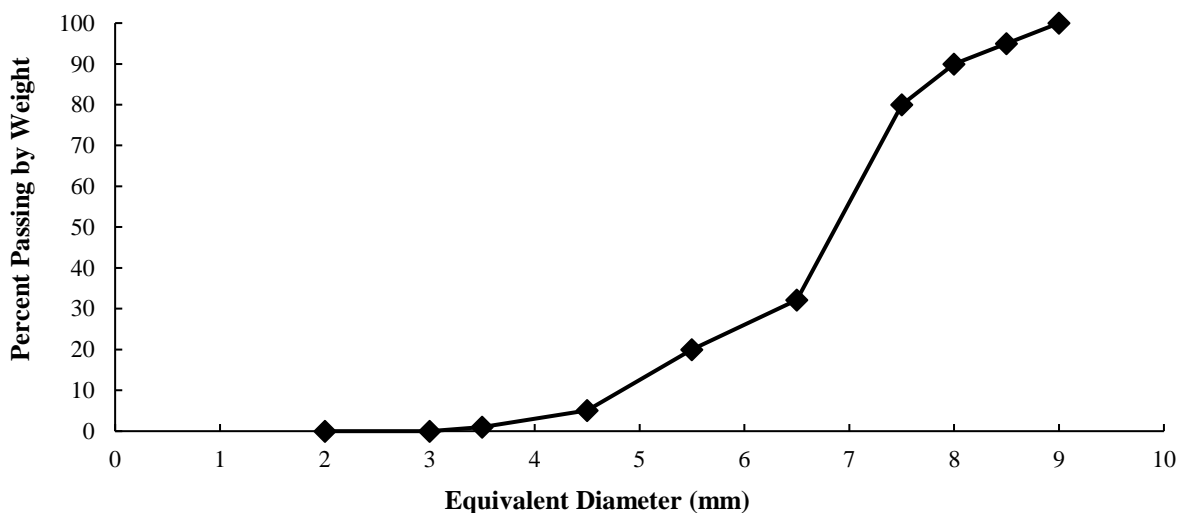


Fig. 4. Grain size distribution used in all simulations

In this research, the diagrams of internal friction angle and volumetric strain against the axial strain are used in order to investigate the mechanical behaviour of the granular assemblies. The sine of mobilised internal friction angle is calculated by:

$$\sin \varphi_{mobilized} = \frac{\sigma_1 - \sigma_3}{\sigma_1 + \sigma_3} \quad (13)$$

where σ_1 and σ_3 : are the major and minor principal stresses, respectively. Also, the volumetric strain of the sample is measured by:

$$\varepsilon_v = \frac{V - V_0}{V_0} \quad (14)$$

where V : is the volume of the cubic cell at a given axial strain, and V_0 : is the initial volume of the sample at the beginning of the sample shearing (i.e., the axial strain of 0.0).

2.5. Different Stages of True Triaxial Test Simulations

A complete simulation of a true triaxial test using the GRANULE program is

composed of four main stages as follows:

2.5.1. Sample Compaction

Since the fundamental approach of the GRANULE is to prohibit the overlap between the particles during the generation process, the initially generated assembly of particles has very high porosity. To reduce the porosity of the specimen and to achieve the desired confining stress, after the initial generation of particles, the rigid boundaries (walls) move towards each other at a strain rate of 5.0×10^{-4} . By doing this, the walls come in contact with the particles and make the granular assembly denser, and at the same time, the stress increases throughout the specimen. This stage continues until the average stress in the specimen slightly exceeds the desired confining stress and the void ratio is between 0.65 and 0.75, the range which was used by Wang and Lade (2001) in their experimental work. Figures 6a and 6b show an example of the sample before and after the compaction, respectively (walls are not shown in these figures).

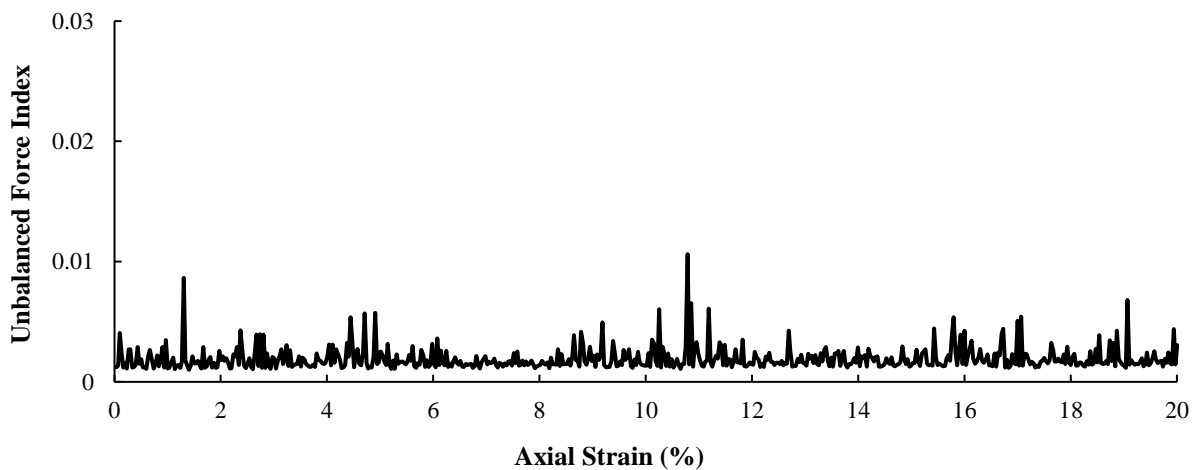


Fig. 5. I_{uf} versus axial strain (ε_a)

Table 2. Values of parameters used in simulations

Parameter	Value
Normal stiffness (N/m)	2.0×10^{10}
Tangential stiffness (N/m)	1.3×10^{10}
Density of particles (N/m ³)	2.65×10^4
Cohesion	0.0
Coefficient of friction between particles	0.5
Coefficient of friction between particles and walls	0.5
Contact damping coefficient	0.1
Global damping coefficient	1.0
Gravity	0.0

2.5.2. Sample Relaxation

At this phase of the test, the velocity of the walls is set to zero. However, particles are not motionless due to the existing contact forces that remained from the compaction stage. This stage continues until the overlap between the particles is minimised. The more cycles are allocated for this phase, the more homogeneity of the sample is reached, leading to a more actual amount of stress within the specimen. At this stage, the porosity of the sample is constant because of the stationary walls, but the stress within the specimen decreases.

2.5.3. Applying the Desired Confining Stress

Once the equilibrium conditions are established, the desired confining stress should be applied to the specimen. This is achieved by a pre-defined servo control in the program. In this process, the required confining stress is compared to the existing stress within the sample. If the existing stress is greater than the desired stress, the walls move away from particles and vice versa. This procedure is repeated for all walls until the existing confining stress is equal to the required stress.

2.5.4. Sample Shearing

After the above-mentioned three phases, the specimen is ready to be tested under the specific requirements of each simulation. For instance, to simulate a triaxial compression test, the stress must be kept constant in two directions (four walls) using the approach explained in the previous phase, and one of (or both) the other two walls move towards the particles at the desired pace (deviatoric strain) in the third direction. This phase continues until the required axial strain (20% in this study) is reached. In the meanwhile, as the wall approaches the particles, the stress increases within the sample as well as in the other two directions. Thus the four walls of those two directions must move away to keep the stress constant and equal to the desired confining stress. This procedure is slightly

different for triaxial tests with a different coefficient (b). Figures 6b and 6c show examples of an assembly of particles under the triaxial compression test at the beginning and the end of the sample shearing, respectively.

3. Results and Discussion

In this section, the results of simulated tests on granular assemblies under general and three-dimensional stress conditions are presented. The purpose of the simulations is to investigate the effect of various factors on the mechanical behaviour of the granular assemblies as well as the shear band characteristics.

In a discrete granular assembly, the interactions between particles occur at the inter-particle contacts, which resist system deformation and maintain stability. Therefore, the macro deformations of the granular assembly are produced because of deformations (or failures) of the initial inter-particle contacts. These contact deformations are considered micro deformations of the system. The normal and tangential deformations, sliding, rolling, and twisting (as well as the combination of them) between two particles at the contact area are thought of collectively as contact deformations and are usually presented in the form of relative displacement increments (Cundall, 1989). In the general 3D case, the mutual configuration of two particles has six degrees of freedom just like a beam in 3D space. In the current analysis, three potential modes of contact displacement: pure rolling, pure sliding, and simultaneous rolling and sliding are considered. Bardet and Proubet (1991) have shown in their study that the particles inside the shear band experience a high degree of rotation and the gradient of particle movement changes near the shear bands. Similarly, in the current study, shear bands are detected employing particle rotation distribution and tracking particle positions throughout the sample shearing.

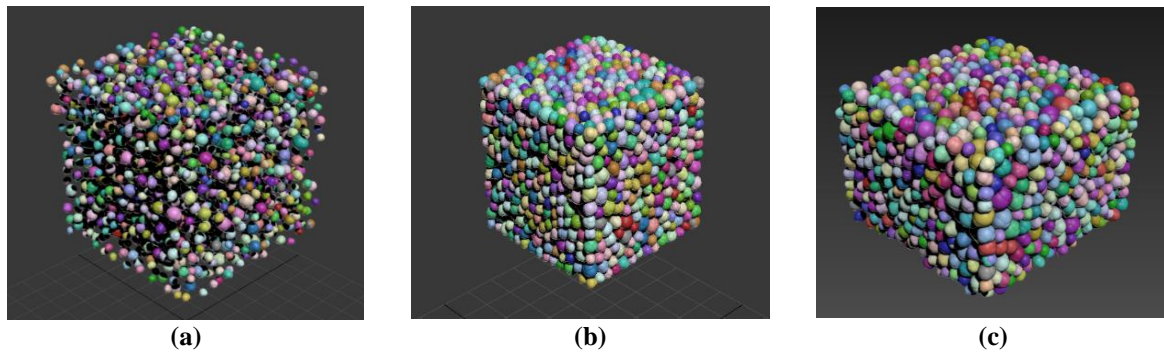


Fig. 6. The assembly of particles: a) Before the compaction; b) After the compaction; and c) At the end of the sample shearing

Due to the complexity of displaying in the 3D environment, the particle rotation distribution is plotted in a set of 2D views (i.e., the X_1 - X_2 , X_1 - X_3 , and X_2 - X_3 views). In all simulations, the direction in which the increasing axial strain as well as the major principal stress (σ_1) were applied, is called X_1 , the one regarding the minor principal stress (σ_3) is X_3 and the other direction would be X_2 . An example of particles rotation distribution and particles displacement plot can be seen in Figures 7a and 7b, respectively, in which the coordinates of the centre of circles represent the initial coordinates of the centre mass of the respective particles and the diameter is a function of the amount of rotation in the direction perpendicular to the proposed view. Therefore, to detect the shear band, an average line passing through the circles with relatively large diameters (distinguished with pink colour) was drawn. The angle of this line with the direction of the minor principal stress (horizontal line)

was considered as the shear band orientation.

3.1. Evaluating the Effect of Intermediate Principal Stress (Coefficient b)

To evaluate the effect of the intermediate principal stress, the b value is used. To this end, five tests with b values of 0.0, 0.25, 0.5, 0.75, and 1.0 with the same initial conditions and confining stress (100 kPa) were simulated. The diagram of the mobilised internal friction angle versus axial strain for the conducted tests is shown in Figure 8a. To better observe and compare the trend of changes in the maximum mobilised internal friction angle against b values, Figure 9 is plotted. As can be seen in this diagram, the maximum mobilised internal friction angle increases as the b value goes from zero to about 0.5 and then decreases for b values between 0.5 and 1.0, which is qualitatively in good agreement with the experimental results obtained by Ochiai and Lade (1983).

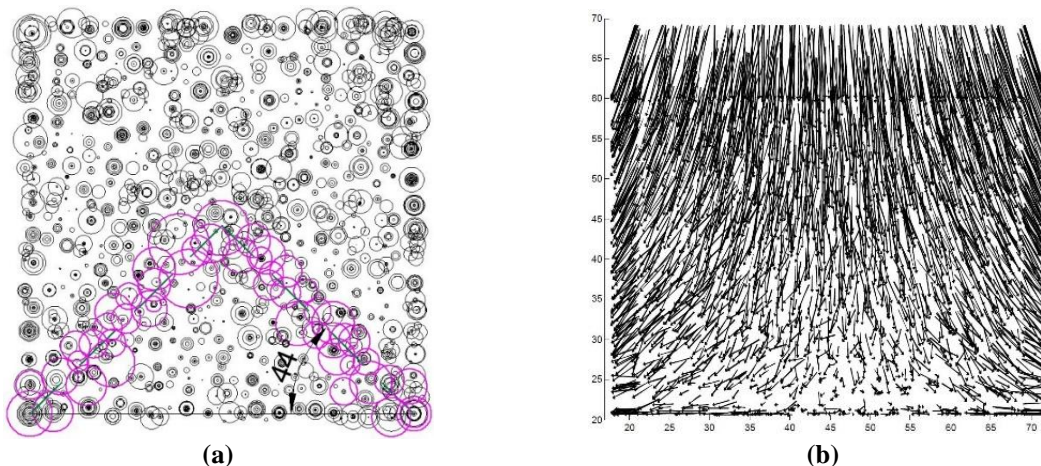


Fig. 7. a) Particles rotation distribution plot; and b) particle displacement plot (X_1 - X_3 view)

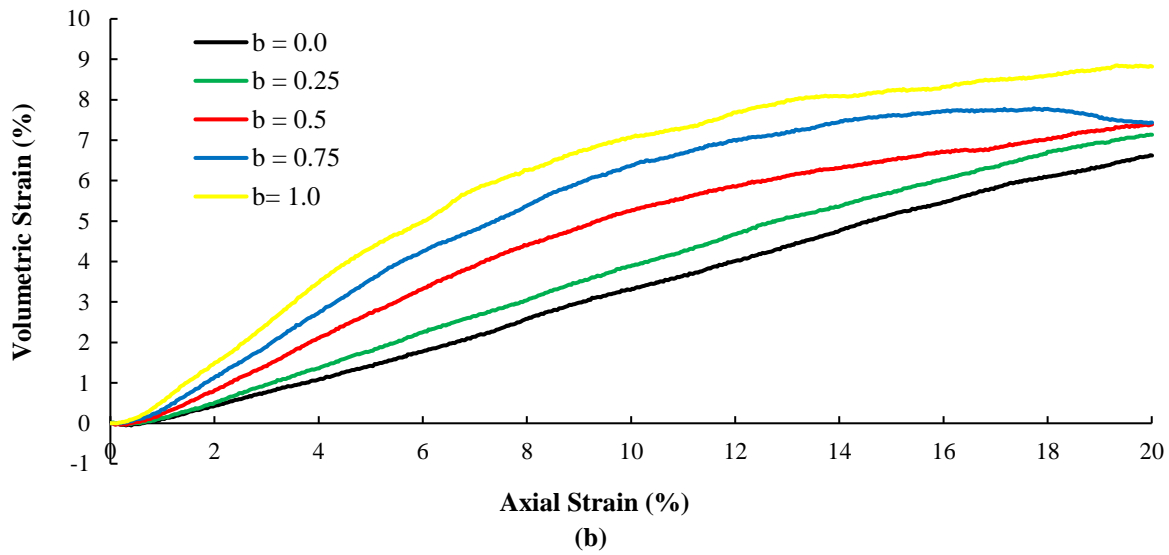
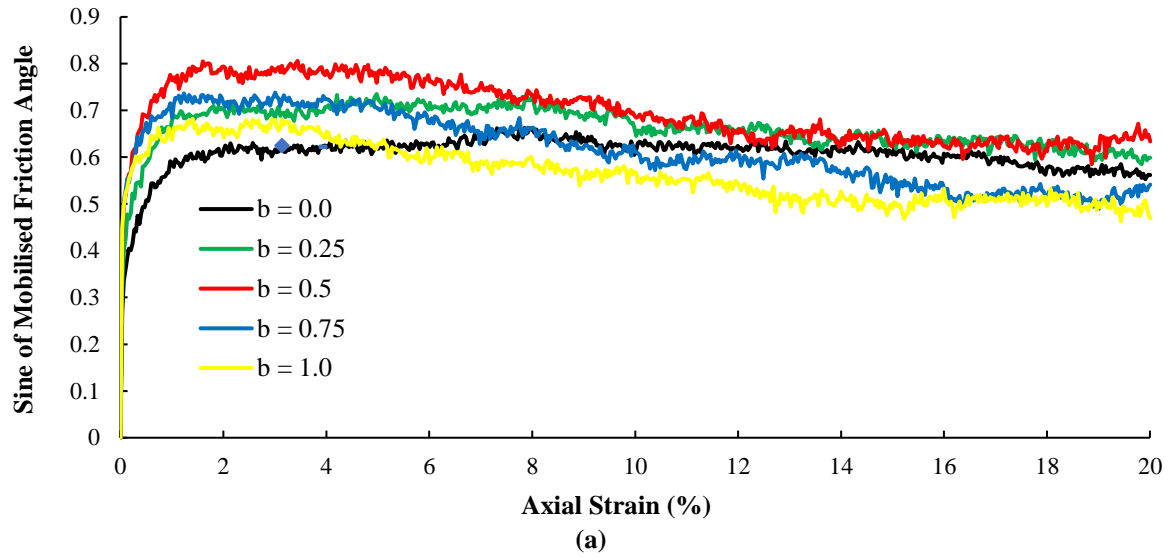


Fig. 8. a) $\sin \varphi_{mobilized}$ versus axial strain (ϵ_a); and b) volumetric strain (ϵ_v) versus axial strain (ϵ_a) for different b values

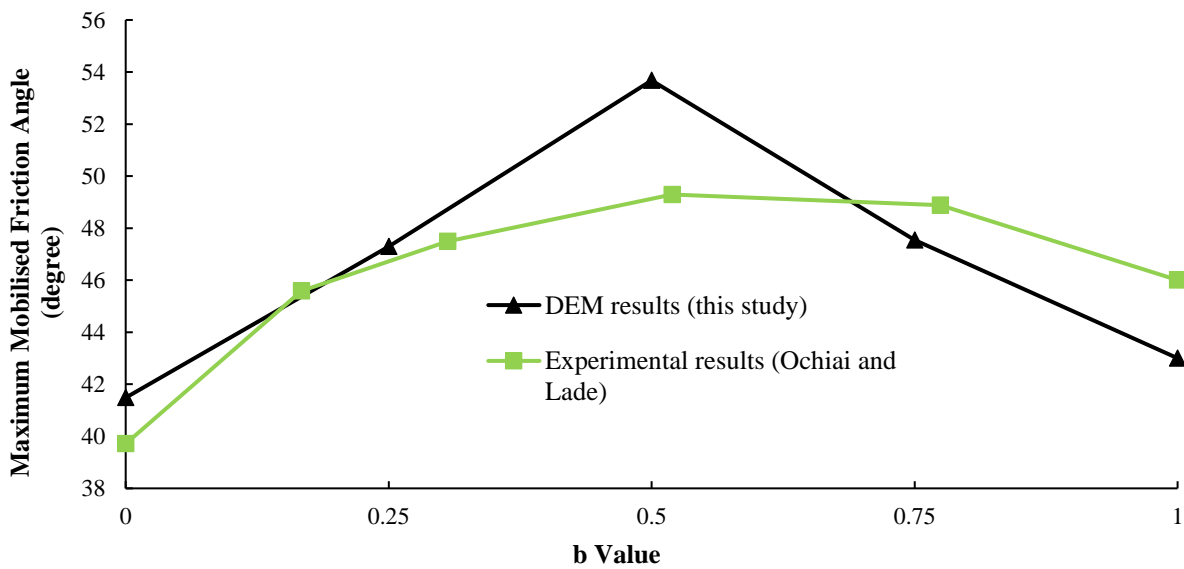


Fig. 9. Comparison of Maximum $\varphi_{mobilized}$ obtained for different b values between experimental results (Ochiai and Lade, 1983) and DEM results (present study)

As indicated in Figure 8b, The more the b value is the more dilation of the sample will be, which is in complete agreement with the similar experimental observations by past researchers such as Rodriguez and Lade (2013). The particle displacement plots in three views for different b values are shown in Figure 10. In order to truncate the process of comparison and evaluation of shear bands, only the results regarding the b value of 0.0, 0.5, and 1.0 are presented. As can be seen in these plots, for b value of 0.0, it seems that the shear band is formed and detectable in both X_1 - X_3 and X_2 - X_3 views (, and possibly with the same formation due to the symmetry in the loading condition and the geometry), while for other b values, the shear band is observed only in the X_1 - X_3 view. Thus, the 3D configuration of the shear band could be considered as a

pyramidal shape for $b=0.0$ and a prism-like shape for other b values as illustrated in Figures 11a and 11b, respectively. This transition from pyramidal shape to prism-like shape configuration is mainly because when b increases, the symmetry in loading condition in both X_1 and X_2 directions is no longer the case and as a result, one pair of walls move away from the particles faster.

In order to determine the inclination of the shear band, the rotation distribution of the X_1 - X_3 view as in Figure 12 was used. The measured orientations for all tests with different b values are summarised in Figure 13. It can be seen that the orientation of shear bands generally increases as the b value increases from 0.0 to 1.0, which is consistent with the experimental results acquired by Lade and Wang (2001).

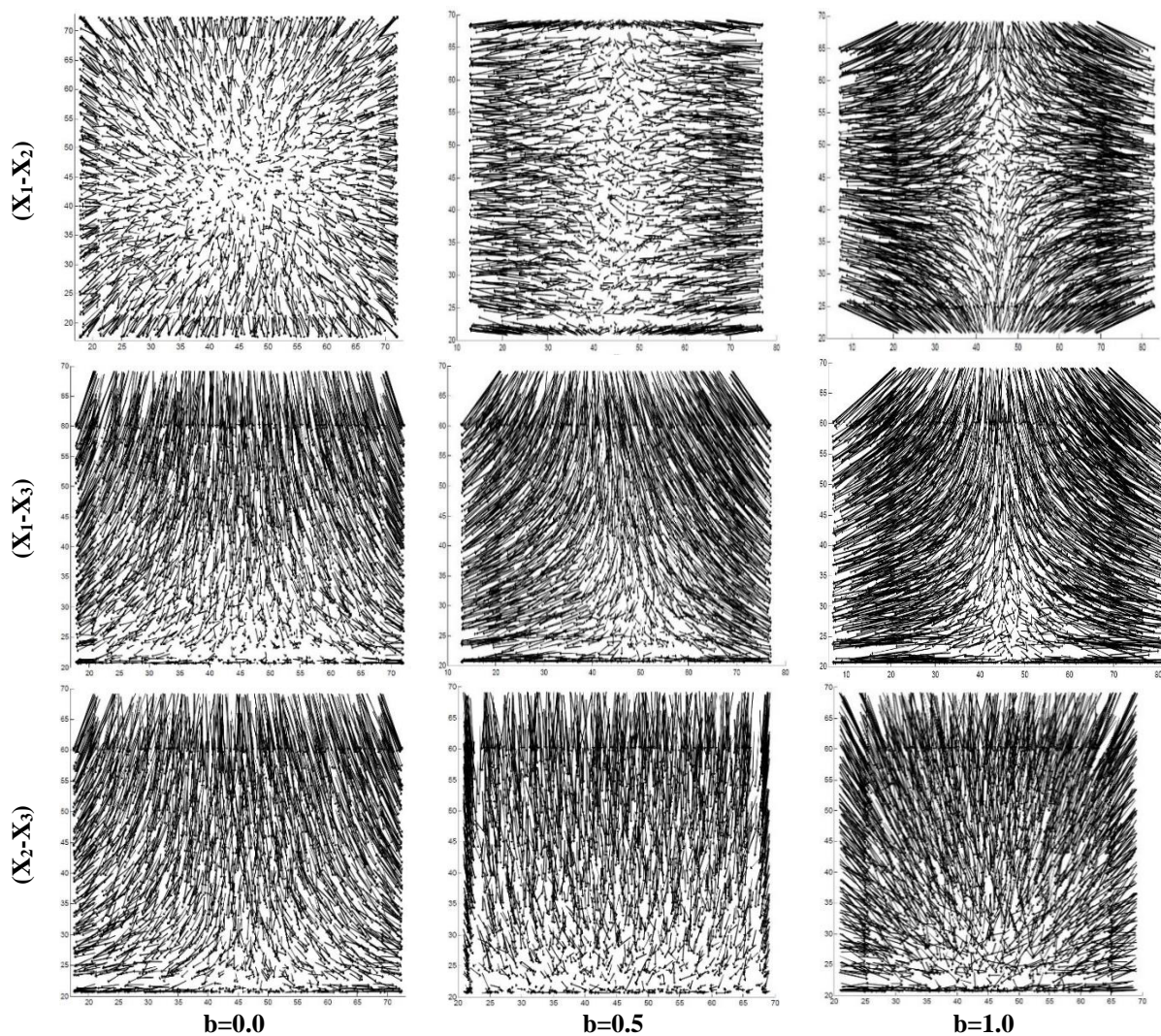


Fig. 10. Particle displacement plot for different b values in three 2D views ($\epsilon_a = 20\%$)

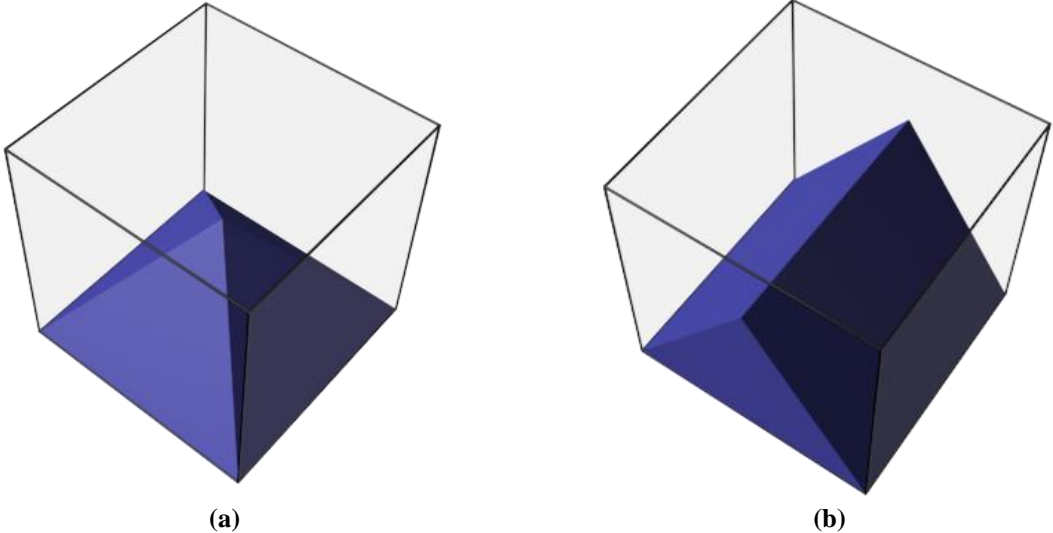


Fig. 11. 3D configuration of the shear bands; a) For b value of 0.0; and b) For other b values

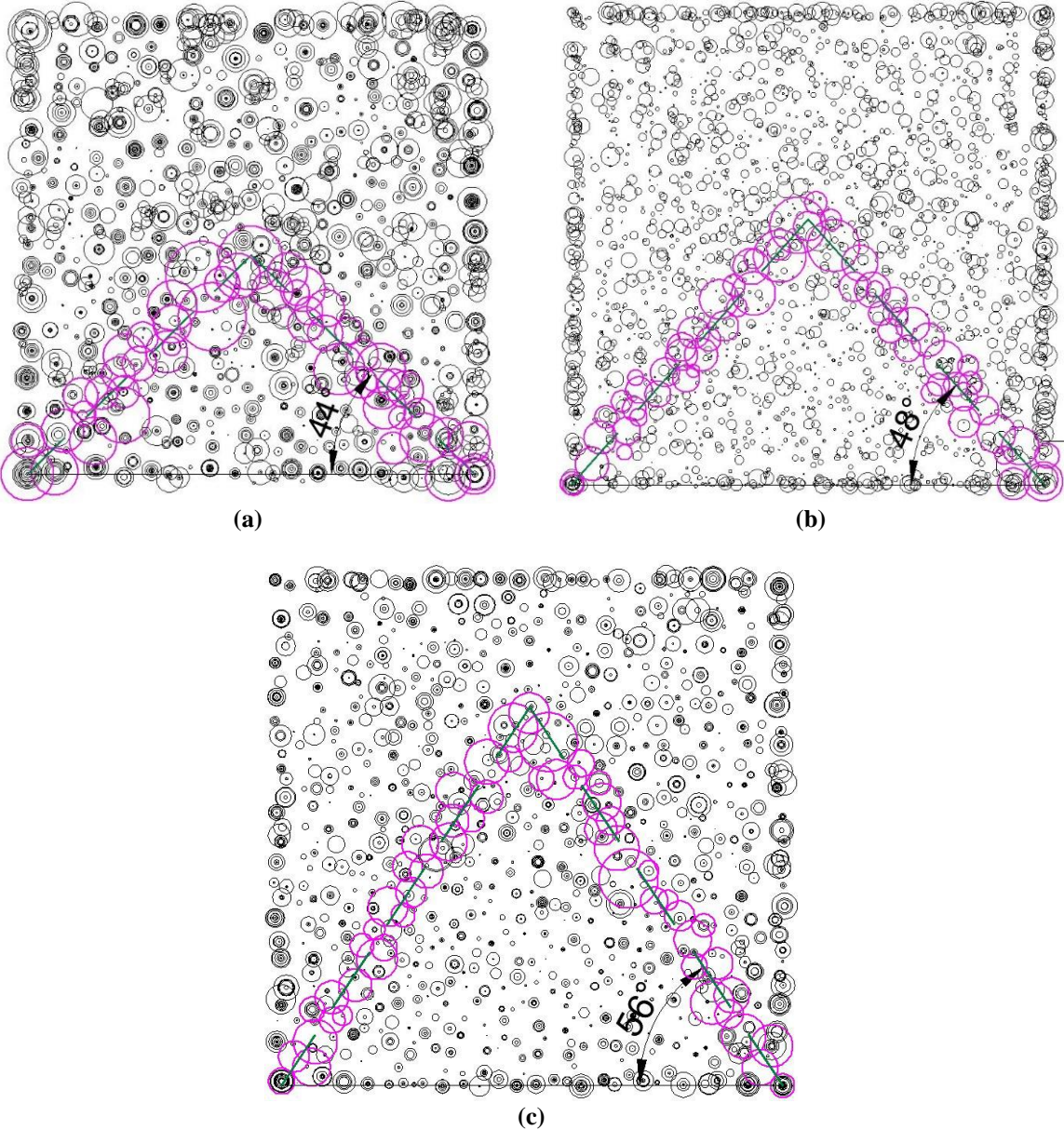


Fig. 12. Particle rotation distribution and shear band inclination: a) $b=0.0$; b) $b=0.5$; and c) $b=1.0$ ($\epsilon_a = 20\%$)

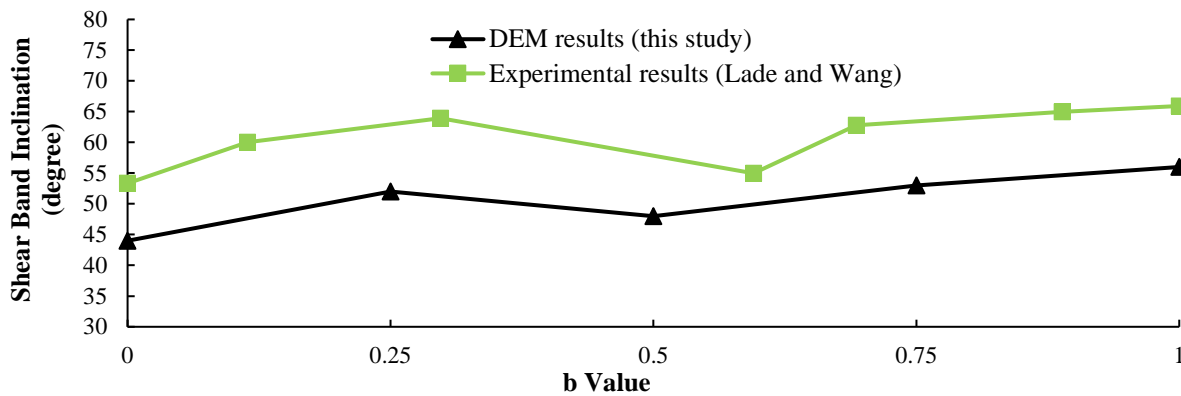


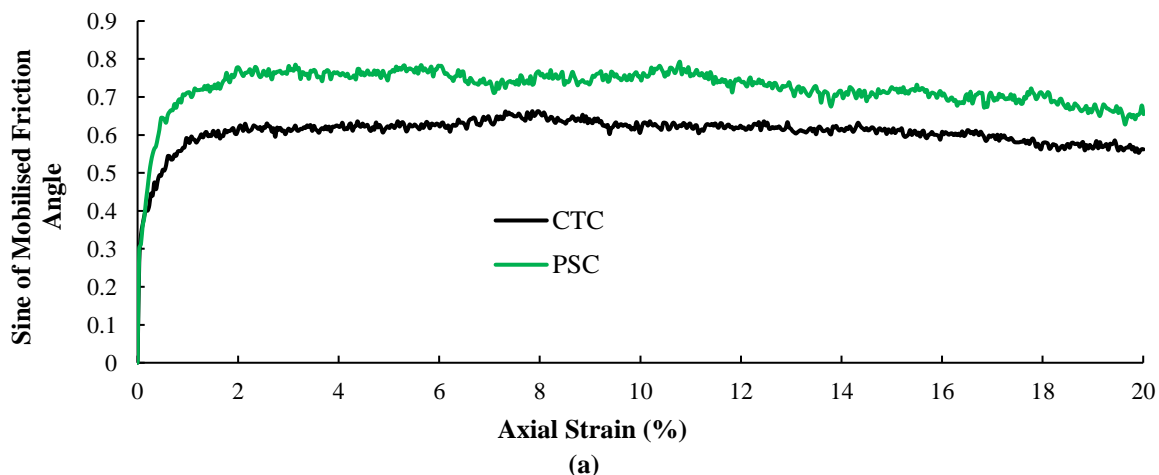
Fig. 13. Comparison of shear band inclination measured for different b values between DEM results (present study) and Experimental results (Lade and Wang, 2001)

3.2. Comparing Plane Strain (PSC) with Compression Triaxial Condition (CTC)

There are some studies regarding the investigation of the shear band in a plane strain condition like what Wang et al. (2019) have carried out. However, most of these studies are in the biaxial condition using 2D simulations. In the current study, a 3D plane strain (PSC) simulation is conducted, and the results regarding the shear band and the mechanical behaviour of the granular assembly was compared to that of Compression Triaxial Condition (CTC). Both simulations were carried out on the samples containing P2-type particles with the same initial arrangements including a confining pressure of 100 kPa and an initial void ratio of 0.643. As can be seen in Figures 14a and 14b, both the internal friction angle and the volumetric strain of the PSC test are considerably higher than that of the CTC test. The increase in the internal friction angle and the dilation can be attributed to the b value of the

simulations. The b value of the PSC simulation was continuously extracted throughout the sample shearing and was plotted as in Figure 15. As can be seen in this figure, the b value of the PSC test is mostly around 0.3. Therefore, the behaviour of the PSC sample is expected to be close to the sample with $b = 0.25$. Thus, based on what was concluded in the simulations with different b values, it is reasonable that the internal friction angle and the dilation of the PSC test are higher than that of the CTC simulation ($b = 0.0$).

As can be seen in Figure 16, the shear band in the PSC test is observable only in the X_1 - X_3 view while in the CTC test is observed both in X_1 - X_3 and X_2 - X_3 views. Therefore, for the PSC simulation, a prism-like shear band could be perceived in a 3D view (Figure 11b). Also, as can be seen in Figure 17, the inclination of the shear band regarding the PSC test is slightly higher than that of the CTC test.



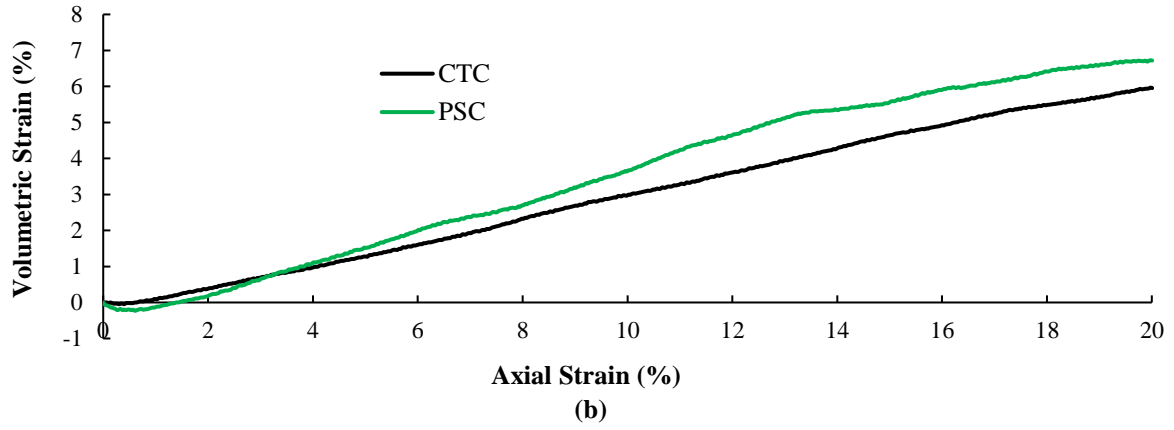


Fig. 14. a) $\sin \phi_{mobilized}$ versus axial strain (ϵ_a); and b) Volumetric strain (ϵ_v) versus axial strain (ϵ_a) for CTC and PSC tests

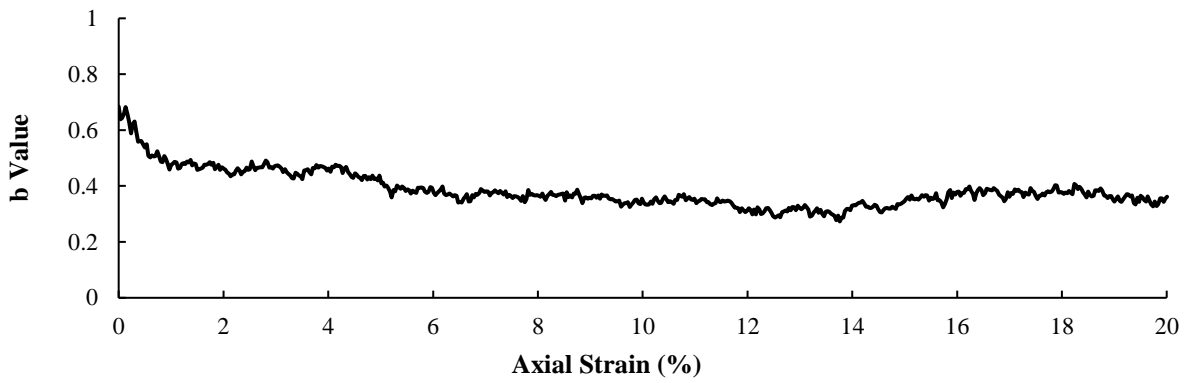
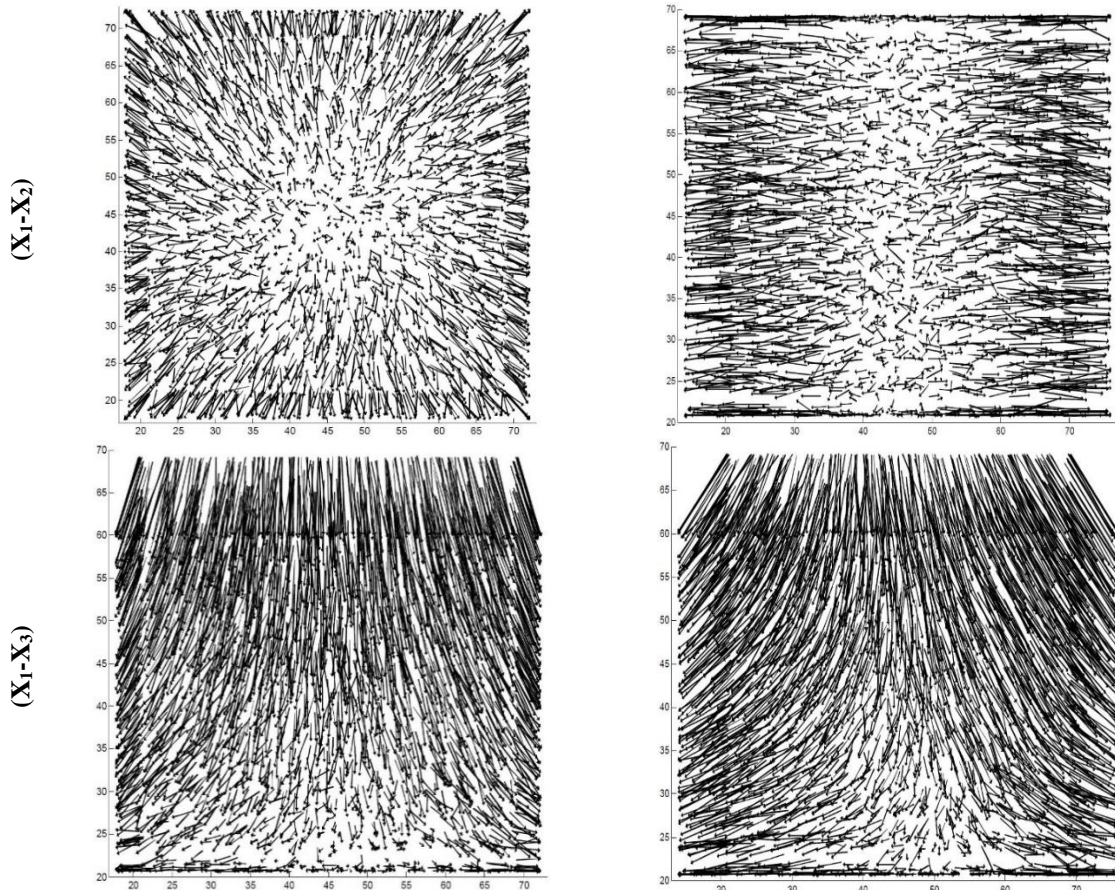


Fig. 15. Measured b value versus axial strain (ϵ_a) for PSC test



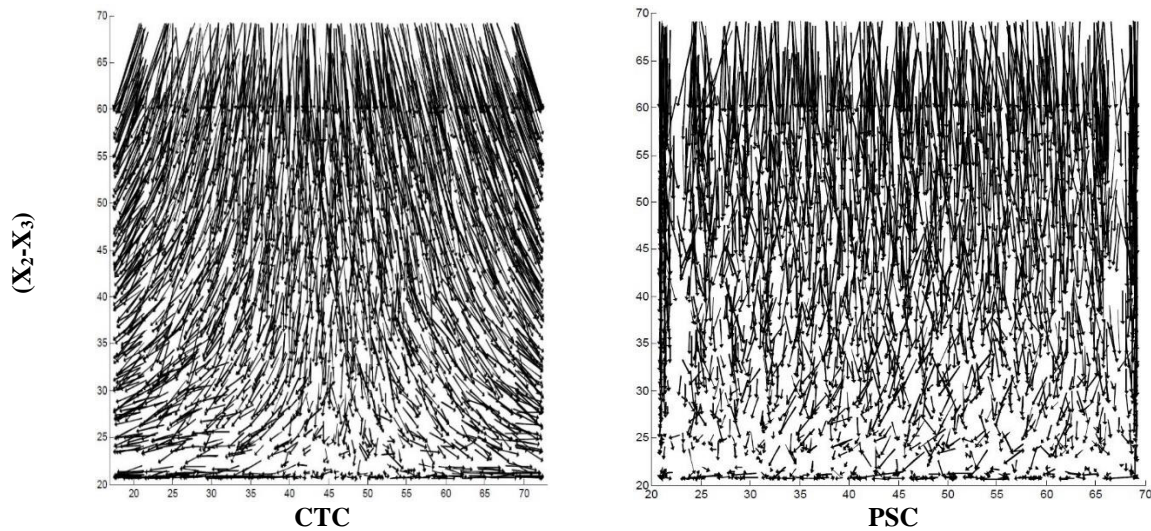


Fig. 16. Particle displacement plot for PSC and CTC tests in three 2D views ($\varepsilon_a = 20\%$)

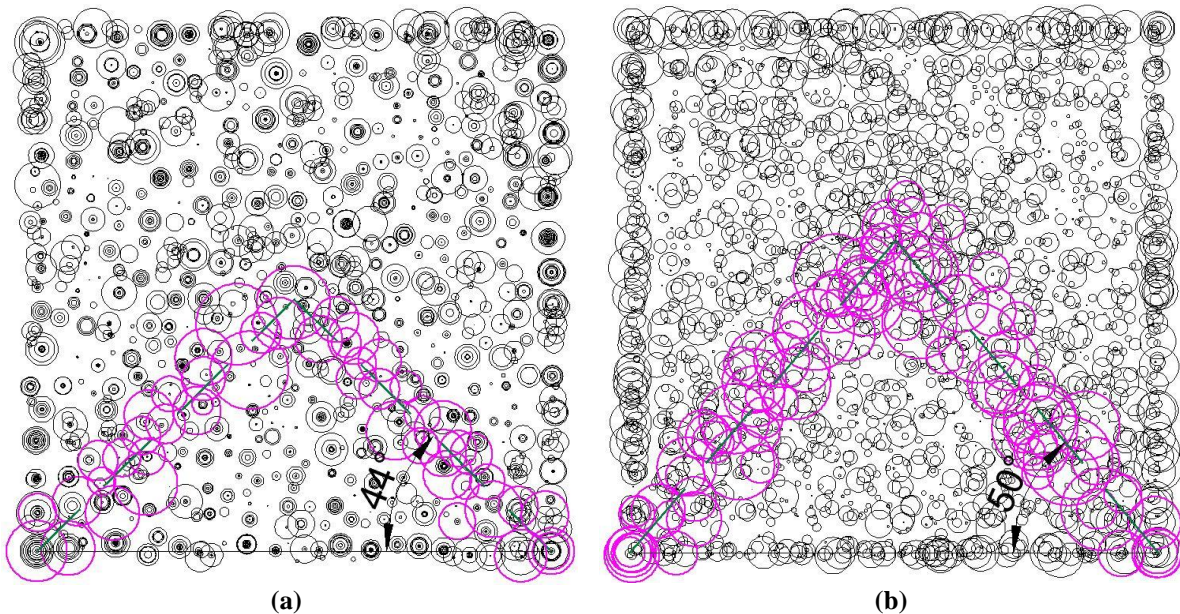


Fig. 17. Particle rotation distribution and shear band inclination: a) CTC test; and b) PSC test ($\varepsilon_a = 20\%$)

3.3. Investigation of the Effect of Particle Shape

To examine the effect of particle shape on the shear band and the mechanical behaviour of the granular assembly, three types of particles, as indicated in Table 1, were used. A set of true triaxial simulations with the same initial arrangements, i.e., $b = 0.5$, and an initial porosity ratio of 0.64 was carried out. As can be seen in Figure 18a, the higher internal friction angle is achieved as the angularity (AI) increases and the sphericity (SPH) decreases. Moreover, the sample containing particles with higher AI and lower SPH shows more dilative behaviour, as shown in Figure 18b. This is

because the interlocking of particles increases substantially when the angularity increases and the sphericity decreases, resulting in more rolling resistance. Additionally, the increase in the maximum internal friction angle can be attributed to the increase in the coordination number. The coordination number is defined as the number of contacts per particle for a set of particles. There are several relationships for the coordination number. In this study the equation proposed by Thornton (2000), which is called the mechanical coordination number was used as follows:

$$Z_m = 2 \frac{N_c - N_p^1}{N_p - (N_p^1 - N_p^0)} \quad (15)$$

where, N_p and N_c : are the total number of particles and contacts, and N_p^0 and N_p^1 : are the number of particles with zero and one contact, respectively. As can be seen in Figure 19, the mechanical coordination number for the assemblies with non-spherical particles is considerably higher than for the spherical package, leading to a higher number of contacts and following that, achieving a higher level of stress in the sample. This increase in stress results in a higher internal friction angle.

As mentioned earlier, for the b value of 0.5, the shear band is only observed in the X_1 - X_3 view. Therefore, the rotation distribution of the X_1 - X_3 view was plotted for these three simulations. It is apparent from Figure 20 that as the angularity increases and sphericity decreases, shear bands with higher inclination are observed.

3.4. Evaluation of the Effect of Confining Stress

To do this, three compression triaxial

tests ($b = 0.0$) with confining stresses of 100, 500, and 1000 kPa were performed. The P2-type particle was used and all other parameters of these tests were considered the same. It can be seen from Figures 21a and 21b that as the confining stress of the samples increases, the mobilised internal friction angle and the dilation of the sample decreases. These observations are qualitatively in good agreement with the typical laboratory results using the compression triaxial device (Kolymbas and Wu, 1990). As mentioned above, in the case of $b = 0.0$, the shear band is formed in both X_1 - X_3 and X_2 - X_3 views, possibly with the same pattern and a 3D pyramidal shape like Figure 11a. Thus the X_1 - X_3 view of the rotation distribution is used to examine the effect of confining stress on the shear band angle. Figure 22 indicates that the increase in the confining stress of the samples results in the decrease of the shear band orientation which is qualitatively consistent with the observed trend in experiments by Han and Drescher (1993) and in DEM simulations by Gu et al. (2014).

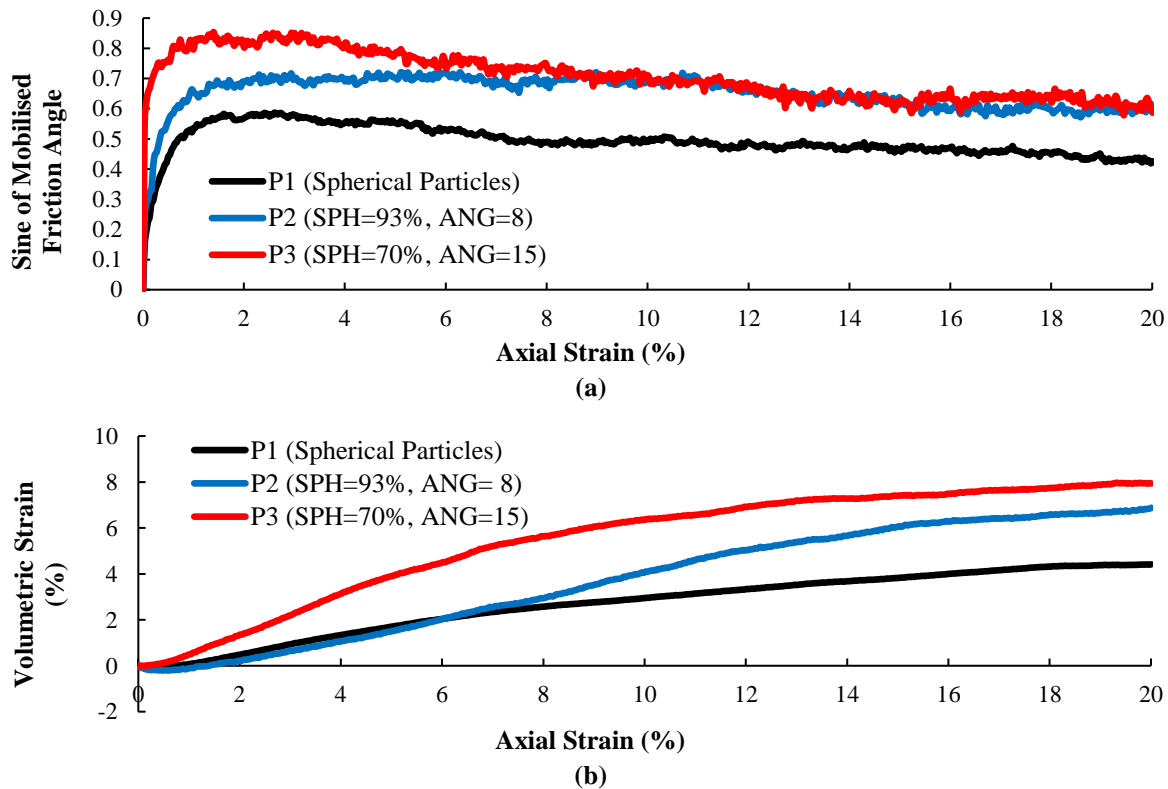


Fig. 18. a) $\sin \varphi_{mobilized}$ versus axial strain (ϵ_a); and b) Volumetric strain (ϵ_v) versus axial strain (ϵ_a) for different particle shapes ($b = 0.5$)

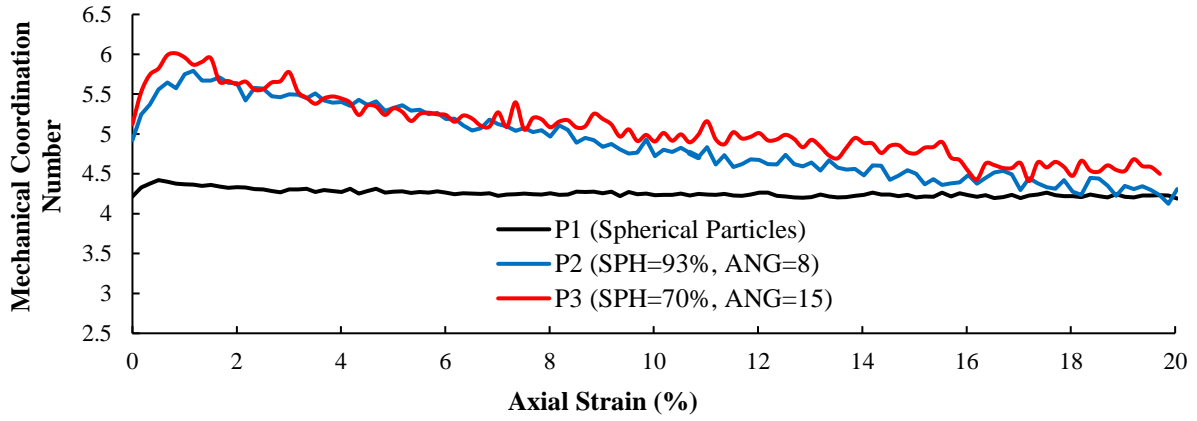


Fig. 19. Mechanical coordination number (Z_m) versus axial strain (ϵ_a) for different particle shapes ($b = 0.5$)

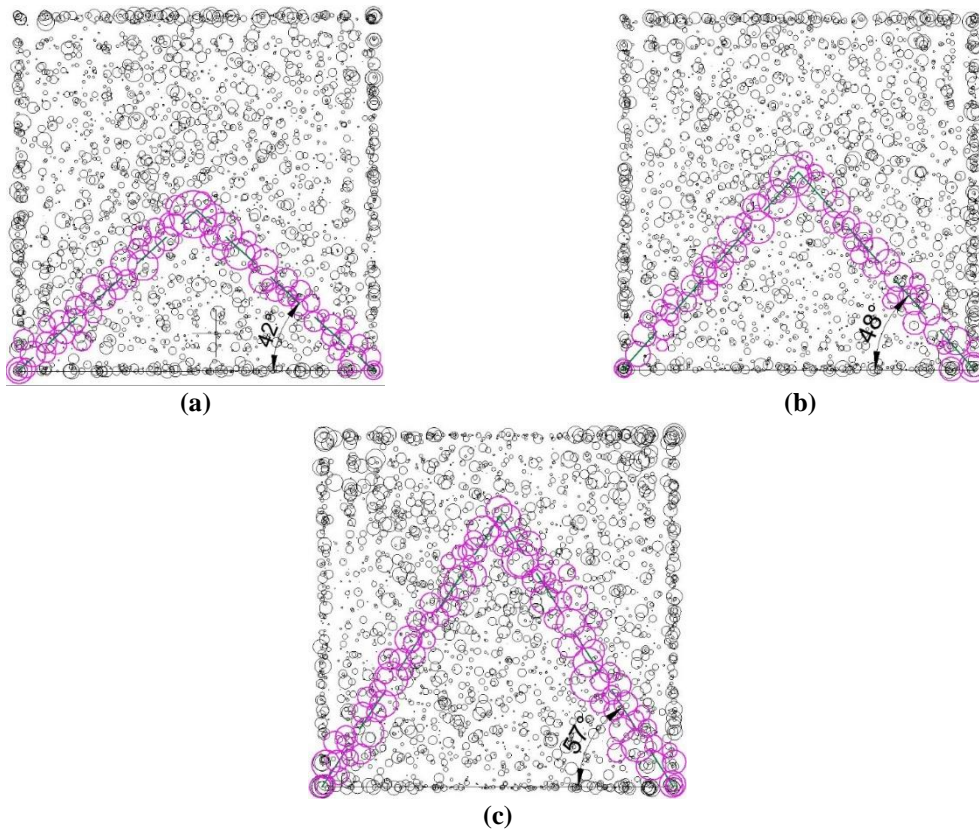
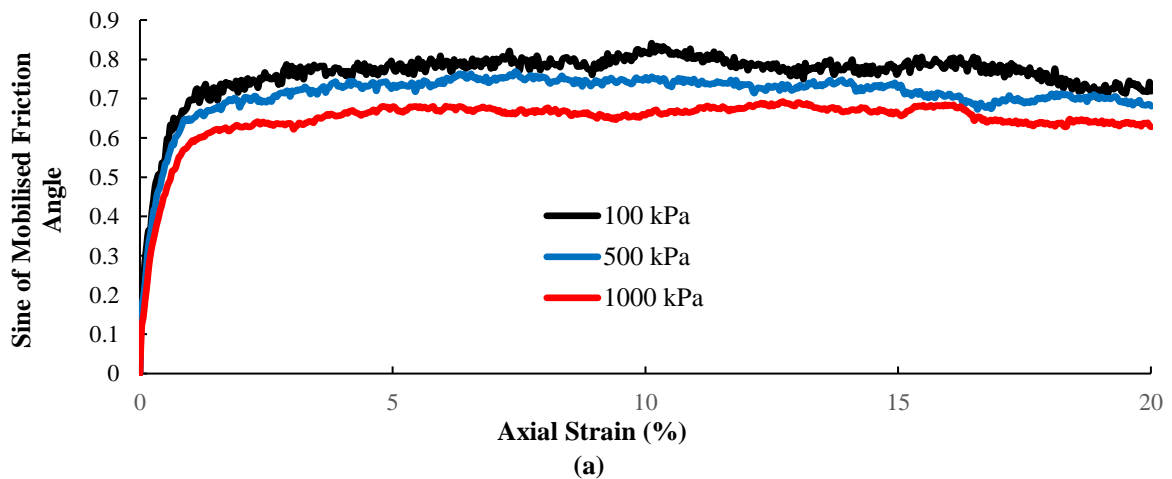


Fig. 20. Particle rotation distribution and shear band inclination in samples with $b = 0.5$ and: a) Spherical particles; b) Particles with AI = 8 and SPH = 93%; and c) Particles with AI = 15 and SPH = 70% ($\epsilon_a = 20\%$)



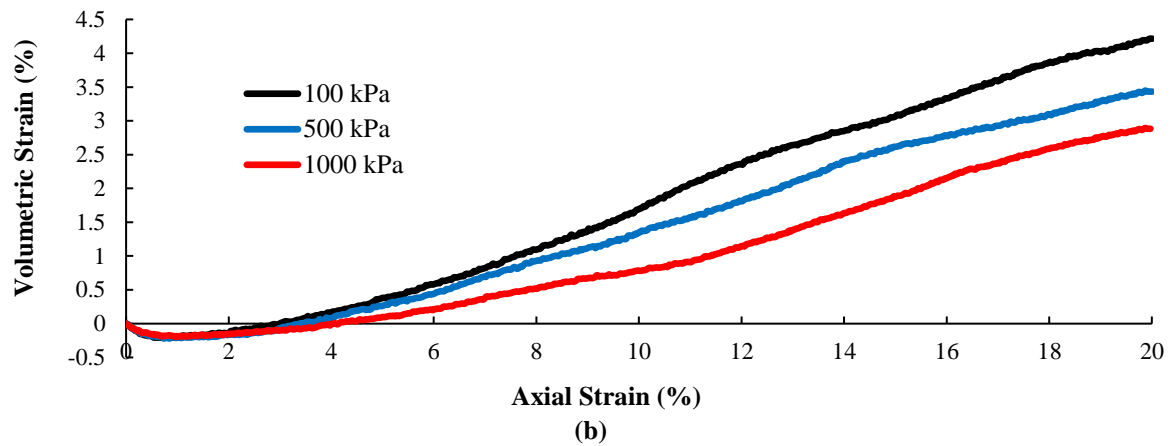


Fig. 21. a) $\sin \varphi_{mobilized}$ versus axial strain (ε_a); and b) Volumetric strain (ε_v) versus axial strain (ε_a) for different confining stresses ($b = 0$)

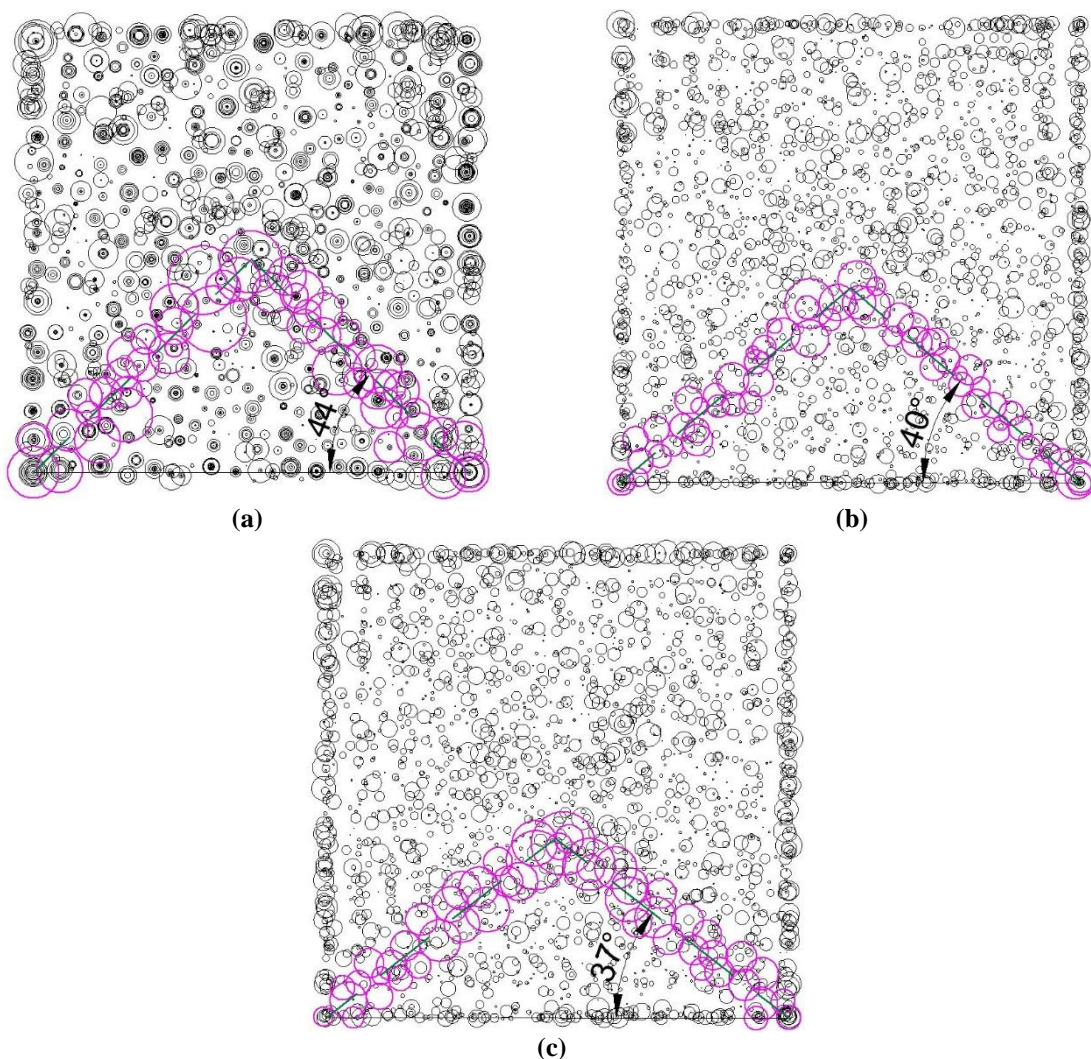


Fig. 22. Particle rotation distribution and shear band inclination in samples with $b=0$ the confining stress of: a) 100 kPa; b) 500 kPa; and c) 1000 kPa ($\varepsilon_a = 20\%$)

4. Conclusions

In this research, the mechanical behaviour of granular materials with emphasis on the pattern and angle of the shear band was

investigated. For this purpose, a three-dimensional discrete element method called GRANULE was used and further developed to include irregularly shaped particles and to simulate tests with different b values.

Then, some systematic simulations were conducted to evaluate the effect of some factors on the mechanical behaviour of the granular assembly and the shear band pattern and orientation. Some acquired results were compared to the past experimental results in order to prove the accuracy and validity of our numerical simulations. The most important results are:

- By increasing the b value from 0.0 to about 0.5, the maximum internal friction angle increases and then decreases for the b value between 0.5 and 1.0 to a value. Moreover, the continuous rise in the b value results in more dilative behaviour of the sample.
- The more the b value is, the more inclination of the shear band will be. However, the shear band angle of the $b = 0.5$ was obtained slightly lower than that of $b = 0.25$.
- The amount of internal friction angle, as well as the dilation of the granular assembly, increases under Plane Strain Condition (PSC) compared to Compressive Triaxial Conditions (CTC).
- The shear band in the PSC test was inclined at a greater angle in comparison to the CTC test.
- It was shown that by reducing the sphericity (SPH) and increasing the angularity (AI) the shear band orientation will rise.
- Considering all the simulations with different conditions, it was concluded that the 3D shape and formation of the shear band is affected only by the change in the b value. In other words, for the simulation with $b = 0.0$ (compression triaxial test), a shear band was observed in both X_1 - X_3 and X_2 - X_3 views with a similar pattern due to the symmetry of the geometry and loading condition, making a pyramidal shape of the 3D shear band. In the case of other b values (and also the PSC test), the shear band is detectable only in the 2D view which is perpendicular to the mean principal

stress (X_1 - X_3 in this study) and a 3D prism-like shear band can be perceived.

5. Disclosure Statement

The authors declare that they have no conflict of interest.

6. References

- Alipour, M.J. and Lashkari, A. (2018). "Sand instability under constant shear drained stress path", *International Journal of Solids and Structures*, 150, 66-82.
- Andrade, J.E., Chen, Q., Le, P.H., Avila, C.F. and Evans, T.M. (2012). "On the rheology of dilative granular media: Bridging solid-and fluid-like behavior", *Journal of the Mechanics and Physics of Solids*, 60(6), 1122-1136.
- Angelidakis, V., Nadimi, S., Otsubo, M. and Utili, S. (2021a). "CLUMP: A Code Library to generate Universal Multi-sphere Particles", *SoftwareX*, 15, 100735.
- Angelidakis, V., Nadimi, S. and Utili, S. (2021b). "SHape Analyser for Particle Engineering (SHAPE): Seamless characterisation and simplification of particle morphology from imaging data", *Computer Physics Communications*, 265, 107983.
- Bardet, J.-P. and Proubet, J. (1991). "A numerical investigation of the structure of persistent shear bands in granular media", *Geotechnique*, 41(4), 599-613.
- Bayesteh, H. and Hoseini, A. (2021). "Effect of mechanical and electro-chemical contacts on the particle orientation of clay minerals during swelling and sedimentation: A DEM simulation", *Computers and Geotechnics*, 130, 103913.
- Chantawarangul, K. (1994). "Numerical simulations of three-dimensional granular assemblies", PhD Thesis, University of Waterloo.
- Cundall, P.A. (1989). "Evolution of elastic moduli in a deforming granular assembly", *S ELECTE*, 59.
- Cundall, P.A. and Strack, O.D.L. (1979). "A discrete numerical model for granular assemblies", *Geotechnique*, 29(1), 47-65.
- Danesh, A., Mirghasemi, A. A. and Palassi, M. (2020). "Evaluation of particle shape on direct shear mechanical behavior of ballast assembly using discrete element method (DEM)", *Transportation Geotechnics*, 100357.
- Desrues, J. and Viggiani, G. (2004). "Strain localization in sand: an overview of the experimental results obtained in Grenoble using stereophotogrammetry", *International Journal for Numerical and Analytical Methods in Geomechanics*, 28(4), 279-321.
- Fransen, M.P., Langelaar, M. and Schott, D.L.

- (2021). "Application of DEM-based metamodelling in bulk handling equipment design: Methodology and DEM case study", *Powder Technology*, 393, 205-218.
- Garcia, F.E. and Bray, J.D. (2019). "Modeling the shear response of granular materials with discrete element assemblages of sphere-clusters", *Computers and Geotechnics*, 106, 99-107.
- Ghassemi, A. and Shahebrahimi, S.S. (2020). "Discrete Element Modeling of Dynamic Compaction with Different Tamping Condition", *Civil Engineering Infrastructures Journal*, 53(1), 173-188.
- Gu, X., Huang, M. and Qian, J. (2014). "Discrete element modeling of shear band in granular materials", *Theoretical and Applied Fracture Mechanics*, 72, 37-49.
- Hajiazizi, M. and Nasiri, M. (2019). "Experimental and numerical investigation of reinforced sand slope using geogird encased stone column", *Civil Engineering Infrastructures Journal*, 52(1), 85-100.
- Han, C. and Drescher, A. (1993). "Shear bands in biaxial tests on dry coarse sand", *Soils and Foundations*, 33(1), 118-132.
- Iwashita, K. and Oda, M. (1998). "Rolling resistance at contacts in simulation of shear band development by DEM", *Journal of Engineering Mechanics*, 124(3), 285-292.
- Jaradat, K.A. and Abdelaziz, S.L. (2019). "On the use of discrete element method for multi-scale assessment of clay behavior", *Computers and Geotechnics*, 112, 329-341.
- Jiang, M., Zhu, H. and Li, X. (2010). "Strain localization analyses of idealized sands in biaxial tests by distinct element method", *Frontiers of Architecture and Civil Engineering in China*, 4(2), 208-222.
- Khabazian, M., Mirghasemi, A.A. and Bayesteh, H. (2020). "Discrete-element simulation of drying effect on the volume and equivalent effective stress of kaolinite", *Géotechnique*, 1-13.
- Kildashti, K., Dong, K., Samali, B., Zheng, Q. and Yu, A. (2018). "Evaluation of contact force models for discrete modelling of ellipsoidal particles", *Chemical Engineering Science*, 177, 1-17.
- Kolymbas, D. and Wu, W. (1990). "Recent results of triaxial tests with granular materials", *Powder Technology*, 60(2), 99-119.
- Krumbein, W.C. (1941). "Measurement and geological significance of shape and roundness of sedimentary particles", *Journal of Sedimentary Research*, 11(2), 64-72.
- Lade, P.V (1978). "Cubical triaxial apparatus for soil testing", *Geotechnical Testing Journal*, 1(2), 93-101.
- Lade, P.V and Wang, Q. (2001). "Analysis of shear banding in true triaxial tests on sand", *Journal of engineering mechanics*, 127(8), 762-768.
- Lashkari, A., Khodadadi, M., Binesh, S.M. and Rahman. M. M. (2019). "Instability of particulate assemblies under constant shear drained stress path: DEM approach", *International Journal of Geomechanics*, 19(6), 4019049.
- Lashkari, A. and Jamali, V. (2021). "Global and local sand-geosynthetic interface behaviour", *Géotechnique*, 71(4), 346-367.
- Mohajeri, M., van Rhee, C. and Schott, D.L. (2018). "Penetration resistance of cohesive iron ore: A DEM study", In *9th International Conference on Conveying and Handling of Particulate Solids*, London.
- Mukherjee, M., Gupta, A. and Prashant, A. (2017). "Instability analysis of sand under undrained biaxial loading with rigid and flexible boundary", *International Journal of Geomechanics*, 17(1), 4016042.
- Nadimi, S., Ghanbarzadeh, A., Neville, A. and Ghadiri, M. (2019). "Effect of particle roughness on the bulk deformation using coupled boundary element and discrete element methods", *Computational Particle Mechanics*, 1-11.
- Ng, T.-T. (2006). "Input parameters of discrete element methods", *Journal of Engineering Mechanics*, 132(7), 723-729.
- O'Sullivan, C. (2011). *Particulate discrete element modelling: A geomechanics perspective*, CRC Press, London.
- Ochiai, H. and Lade, P.V (1983). "Three-dimensional behavior of sand with anisotropic fabric", *Journal of Geotechnical Engineering*, 109(10), 1313-1328.
- Rodriguez, N.M. and Lade, P.V (2013). "True triaxial tests on cross-anisotropic deposits of fine Nevada sand", *International Journal of Geomechanics*, 13(6), 779-793.
- Rudnicki, J.W. and Rice, J.R. (1975). "Conditions for the localization of deformation in pressure-sensitive dilatant materials", *Journal of the Mechanics and Physics of Solids*, 23(6), 371-394.
- Salimi, M.J. and Lashkari, A. (2020). "Undrained true triaxial response of initially anisotropic particulate assemblies using CFM-DEM", *Computers and Geotechnics*, 124, 103509.
- Shamsi, M.M.M. and Mirghasemi, A.A. (2012). "Numerical simulation of 3D semi-real-shaped granular particle assembly", *Powder Technology*, 221, 431-446.
- Sukumaran, B. and Ashmawy, A.K. (2001). "Quantitative characterisation of the geometry of discrete particles", *Geotechnique*, 51(7), 619-627.
- Tang, H., Dong, Y., Wang, T. and Dong, Y. (2019). "Simulation of strain localization with discrete element-Cosserat continuum finite element two scale method for granular materials", *Journal of the Mechanics and Physics of Solids*, 122, 450-471.

- Thornton, C. (2000). "Numerical simulations of deviatoric shear deformation of granular media", *Geotechnique*, 50(1), 43-53.
- Tian, J., Liu, E. and He, C. (2020). "Shear band analysis of granular materials considering effects of particle shape", *Acta Mechanica*, 231(11), 4445-4461.
- Vardoulakis, I. (1989). "Shear-banding and liquefaction in granular materials on the basis of a Cosserat continuum theory", *Ingenieur-Archiv*, 59(2), 106-113.
- Wang, P., Sang, Y., Shao, L. and Guo, X. (2019). "Measurement of the deformation of sand in a plane strain compression experiment using incremental digital image correlation", *Acta Geotechnica*, 14(2), 547-557.
- Wang, Q. and Lade, P.V (2001). "Shear banding in true triaxial tests and its effect on failure in sand", *Journal of Engineering Mechanics*, 127(8), 754-761.
- Yan, Y., Zhao, J. and Ji, S. (2015). "Discrete element analysis of breakage of irregularly shaped railway ballast", *Geomechanics and Geoengineering*, 10(1), 1-9.
- Yu, J., Jia, C., Xu, W., Zhang, Q. and Wu, C.J. (2021). "Granular discrete element simulation of the evolution characteristics of the shear band in soil-rock mixture based on particle rotation analysis", *Environmental Earth Sciences*, 80(6), 1-14.
- Zhao, S. and Zhao, J. (2021). "SudoDEM: Unleashing the predictive power of the discrete element method on simulation for non-spherical granular particles", *Computer Physics Communications*, 259, 107670.



This article is an open-access article distributed under the terms and conditions of the Creative Commons Attribution (CC-BY) license.